STUDY OF THE LEAKAGE TRACER GAS TRANSPORT PROPERTY IN CONDENSER: He and SF_6

Jianfeng Wan [1], Jian Hu [1], Wenyan Bi [2*], Menglin Yu [1], Xiangxuan Xu [1], Yihong Sun [1], Qiang Zhou [2], Yikai Hou [2], Xuemao Guan [2*]

1. School of Mechanical and Power Engineering, Henan Polytechnic University, Jiaozuo, Henan 454000, China; 2. College of Chemistry and Chemical Engineering, Henan Polytechnic University, Jiaozuo, Henan 454000, China; 3. School of Materials Science and Engineering, Henan Polytechnic University, Jiaozuo, Henan 454000, China

Helium (He) tracer method is one of the common methods used to detect tube bundle leakage in the condenser. To improve the detection accuracy, sulfur hexafluoride (SF_6) is considered a tracer gas instead of He. This paper combines the N-S equation, porous medium model, flow diffusion model and steam heat transfer model to develop the numerical model of tube bundle leakage in the condenser. The simulation results show that the transport of leaked gases (He and SF_6) consists of flow and diffusion patterns. The existence of the diffusion process is confirmed further through theoretical analysis. The two gases have the same transport behavior in the pure flow process. When it involves the diffusion process, the flow rate of He is 6.67 times that of SF_6. In other words, the time required for He to reach the same concentration difference is 1/6.67 times that of SF_6. In addition, the influence of leakage intensity and gas species on the transport is analyzed. The study results provide a theoretical basis for SF_6 to replace He as a tracer gas to detect tube bundle leakage.

Key words: *tube bundle, condenser, leakage, porous media model, flow diffusion model, tracer gas method*

*Corresponding author.
E-mail address: biwenyan@hpu.edu.cn (Wenyan Bi)
guanxuemao@hpu.edu.cn (Xuemao Guan）

1 Introduction

Condenser is a common equipment used in nuclear power plants, which plays a vital role in providing hot wells and vacuum for steam turbine exhaust and other extraction [1, 2]. And there are thousands of tube bundles in the condenser. Once the condenser tube bundle develops a leak, it will directly impact the quality of the circulating water, thereby affecting the service life of the steam generator and jeopardizing the safe production of the nuclear power plant [3]. Consequently, it is essential to detect the tube bundle leakage in the condenser regularly. The traditional methods for leakage detection in condensers often require shutting down the systems. These methods have limitations such as long detection time and a lot of resource consumption, which directly impair the economic benefits of the power plant.

A tracer gas detection method has emerged as a high-precision online non-destructive testing technique. This method has significant advantages, such as short testing time, high precision, and low cost. It is widely used in various industries. In the coal industry, tracer gas is used to analyze the ventilation rate for underground mines [4]. In the medical field, tracer gas explores the airborne transmission of respiratory infectious diseases [5]. In the aerospace field, tracer gas is used for optimization research on engine performance [6].

Moreover, the tracer gas detection method can be applied to detect the leakage in the tube bundle of the condenser during operation [7]. Introducing tracer gas into the condenser tube bundle and then inspecting the extraction port’s parameters like concentration and flow rate can determine whether there is a leak in the tube bundle. The different physical and chemical properties of tracer gases will result in variations in sensitivity and efficiency for leak detection [8]. Helium (He) is usually used as the detection gas [9-12], which has the characteristics of being highly stable [13] and pollution-free [14]. However, there are trace amounts of He in the air, meaning that the condenser's non-condensable gases contain He [12, 15]. This may lead to leakage detection errors and decreased sensitivity. Sulfur hexafluoride (SF6) is a non-toxic, non-flammable inert gas whose pressure-temperature relationship follows the ideal gas state equation, similar to He [16, 17], and SF_6 does not exist in the air [18], making it less prone to errors. Therefore, SF_6 is considered as a tracer gas instead of He to improve the detection accuracy.

In addition, many scholars are using various software and hardware to analyze and locate leakage source information [19]. For example, Liang et al. [20] studied the leakage characteristics of natural gas pipelines using a data-driven digital twin method. Zhang et al. [21] analyzed leakage source information based on acoustic emission characteristics. Idachaba et al. [22] inferred leakage source information by installing pressure sensors. However, the flow inside the condenser is complex, and it is challenging to deduce leakage information through low-cost artificial intelligence. Furthermore, according to the condenser's structural characteristics and internal operating conditions, it is difficult to install many hardware devices to detect leakage information. Therefore, it is necessary to analyze leakage information from the flow perspective.

In summary, this paper will investigate the transport characteristics of two gases during leakage in a condenser through flow simulation, thus providing a theoretical basis for using SF_6 as a replacement detection gas for He. According to the actual power plant, the physical model of the condenser is established. The gas leakage process within the condenser is described using the N-S equation, porous

media model, and gas convection-diffusion equation. By employing these mathematical models, this research studies the transport characteristics and behavior of He and SF_6.

2 Physical model

This article takes the condenser of the power plant as the research object. It mainly consists of a throat, heat exchange module (tube bundle zone), hot well, collection tank, flash tank, water chamber, double low-pressure heater, deaerator/pressure reducer, condensate filtration device, condenser extraction steam device, etc. There are four tube bundle zones, each consisting of 14643 titanium tubes with an outer diameter of 25 mm and a length of 16471 mm. To decrease the complexity of the model, we define the four tube bundle zones as a porous medium, labelled as Zone 1, 2, 3, and 4 in fig. 1a. Zones 1 and 2 are located in one steam chamber, while Zones 3 and 4 are in another. Each tube bundle zone is equipped with a steam extraction port and a circulating water pump. The circulating water pump operates in three different states, as illustrated in tab. 1. In this table, the operating condition of "100% TMCR" denotes the turbine's maximum continuous rate, with an inlet flow rate of 371.78 kg/s, cooling water temperature of 24 °C, and condenser back pressure of 5600 Pa.

Tab. 1 Circulating water pump operating condition table.

Operating condition	1, 3- circulating water pump state	2, 4- circulating water pump state
1 and 3 are in operation	open	close
2 and 4 are in operation	close	open
100% TMCR	open	open

Fig. 1a also shows steam and tracer gas's inlet and outlet distribution. The green area in the figure represents the steam inlet, and the red area represents the fluid outlet. The physical model of the condenser has a total of two inlets and four outlets, marked as Inlet 1, Inlet 2, Outlet 1, Outlet 2, Outlet 3, and Outlet 4 in order along the positive X-axis.

Although the position of the leakage point significantly impacts the phenomenon of leakage transport, this study only focused on researching the leakage position in a typical zone to reduce computational complexity and analysis time. This leakage position is located directly above the steam impingement side of the tube bundle, allowing for a better analysis of the tracer gas transport. As depicted in fig. 1a, the blue portion enclosed by the pink dashed line represents the location of the leakage point. For a specific illustration of the leakage point location, it can be referred to fig. 1b, where the blue color represents the leakage position, with a corresponding volume of 0.00894 m^3.

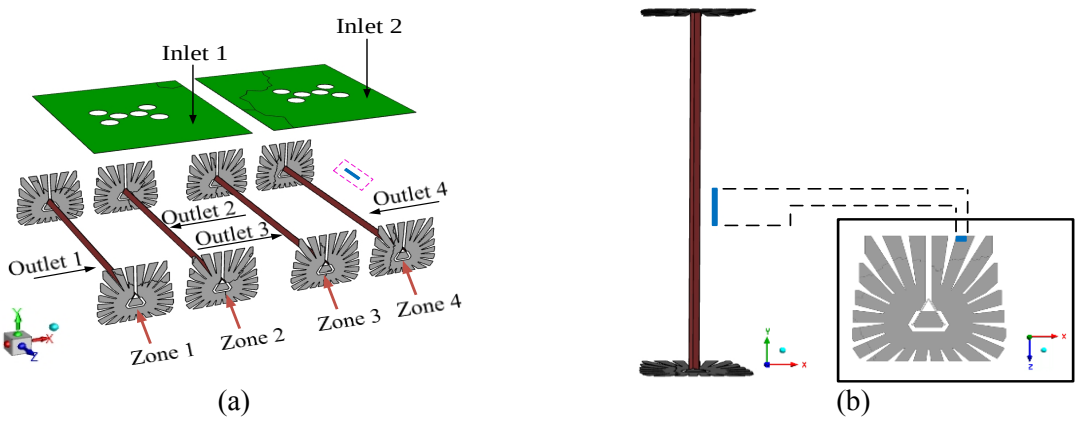

(a) (b)

Fig. 1 The physical model and boundary definition of condenser. (a) The inlet and outlet location. (b) Schematic diagram of leakage point location.

3 Mathematical model

3.1 Model assumption

The condenser system is highly complicated, so it needs to be reasonably simplified to establish the governing equation. The following assumptions are made:

(1) The cooling water flow rate on the tube side is uniformly distributed.

(2) The leaked gas and steam form a uniformly mixed ideal gas, and the steam is saturated.

(3) The volume occupied by the condensate and its interaction with the mixed gas is neglected.

(4) The inlet steam pressure is the same for each steam chamber, and there is an equal pressure drop from the steam inlet to the extraction port.

3.2 Governing equations

For the convenience of program writing, the main governing equations are written in a unified form (eq. (1)). The specific equations are obtained based on tab. 2. In eq. (1), ϕ, Γ_ϕ, and S_ϕ are the substituted variables. β denotes the porosity [23], which is equal to the volume of fluid within the control body divided by the volume of the control body, determined by the dimensions and distribution of the tube bundle. The value of β is zero outside the porous medium tube bundle zone. ρ is the steam density. u, v, and w represent the flow velocities in the x, y, and z directions, respectively. x_a is the mass concentration of the leaked gas. $\dot{m}$ is the condensation rate of vapor per unit volume at the local level. c_a is the diffusion coefficient of the leaked gas [24]. M_a is the mass sink of the leaked gas, which is zero everywhere except at the leak point.

$$\frac{\partial(\beta\rho\phi)}{\partial t}+\frac{\partial(\beta\rho u\phi)}{\partial x}+\frac{\partial(\beta\rho v\phi)}{\partial y}+\frac{\partial(\beta\rho w\phi)}{\partial z}=\frac{\partial}{\partial x}\left(\beta\Gamma_\phi\frac{\partial\phi}{\partial x}\right)+\frac{\partial}{\partial y}\left(\beta\Gamma_\phi\frac{\partial\phi}{\partial y}\right)+\frac{\partial}{\partial z}\left(\beta\Gamma_\phi\frac{\partial\phi}{\partial z}\right)+S_\phi \quad (1)$$

Tab. 2 Specific governing equations table.

Governing equations	ϕ	Γ_ϕ	S_ϕ
Continuity equation	1	-	$-\dot{m}$
Momentum equation in the x direction	u	μ	$-\beta\frac{\partial p}{\partial x}-\beta F_x-\dot{m}u$
Momentum equation in the y direction	v	μ	$-\beta\frac{\partial p}{\partial y}-\beta F_y-\dot{m}v$
Momentum equation in the z direction	w	μ	$-\beta\frac{\partial p}{\partial z}-\beta F_z-\dot{m}w$
Convective diffusion equation of leaked gas [25]	x_a	c_a	$-M_a$

Other variables ($\dot{m}$, F_x, F_y, F_z) are determined by eqs. (2) ~ (5) [26]. Here, $\dot{m}$ represents the condensation rate of steam per unit volume at the local level. Δt_m is the logarithmic mean temperature difference. R_{tot} is the total thermal resistance from the steam side to the waterside. γ is the latent heat of steam condensation at the local level. C_V and C_A represent the thermal volume of the control body and the heat transfer area of the cooling pipe inside the control body, respectively. ξ is a parameter related to the distribution of the tube bundle structure and the direction of the gas, referring to the literature [27] for specific calculation, and U is the steam velocity.

$$\dot{m}=\frac{\Delta t_m C_A}{R_{tot}\gamma C_V} \tag{2}$$

$$F_x=\xi\rho uU \tag{3}$$

$$F_y=\xi\rho vU \tag{4}$$

$$F_z=\xi\rho wU \tag{5}$$

There are another six unknown variables (ρ, p, u, v, w, x_a) in the above equations, and an additional ideal gas state equation is presented (eq. (6)) [28]. Here, p represents the steam pressure, T represents the steam temperature, and R represents the gas constant of steam.

$$\rho=\frac{p}{RT} \tag{6}$$

3.3 Boundary conditions

The boundary conditions are set according to the actual operating conditions of the condenser in the LingAo Phase II Nuclear Power Plant. The mass flow rate of steam is selected as the velocity inlet. The pressure outlet is set to simulate the steam extraction from the condenser outlet. The specific operating conditions are as follows: steam flow rate at inlet is 241.855 kg/s, exhaust pressure is 6700 Pa, working pressure is 6700 Pa, circulating water temperature is 24 ℃, circulating water velocity is 2.38 m/s, and circulating water pumps 1 and 3 are in operation.

In addition, the RNG $k-\varepsilon$ turbulence model [29] is adopted. The standard wall function is employed for near-wall treatment in steady-state simulation. After completing the steady-state simulation, the obtained results are utilized as initial conditions for the subsequent transient

simulation. The time step size is set to 0.015 s, and the maximum number of iterations per time step is 50.

4. Grids independence test and model validation

4.1 Grids independence test

To reduce grid complexity, this paper introduces a hybrid grid approach. Within the tube bundle zone, a two-dimensional quadrilateral grid forms a cross-section, which are then swept along the bundle direction. Outside the tube bundle zone, an unstructured grid is employed. Under 100 % TMCR operating condition, steady-state calculations were performed for four grid quantities: 473520, 534633, 638228 and 721352. The results indicate that the steam extraction port's deviation in steam flow rate is less than 5 % for all grid configurations. To save computational resources, the simulation in this paper continues using the grid quantity of 638228.

4.2 Validation of the model

To verify the model's accuracy, transient simulation was performed using the 100 % TMCR operating condition. The simulation yielded the steam outlet parameter values of 34.81 ℃ for temperature and 3434.7 Pa for pressure. The on-site operation at the nuclear power plant under the same conditions recorded temperature and pressure values of 35.01 ℃ and 3466 Pa, respectively. Comparatively, the deviations between the simulated and actual values for both parameters are less than 5 %. In this operating condition, the valve connecting the low-pressure heater to the condenser pipe was opened and the He cylinder was attached. The valve opening was kept as small as possible to ensure a very low flow rate. After a few minutes, the concentration of He at each extraction port was measured when it reached its peak. By comparing the concentration between the four outlets, it is found that the ratio value is 21:57:0:0 (Outlet1: Outlet2: Outlet3: Outlet4). Then, the valve opening was adjusted and a second measurement of the concentration was performed, obtaining the ratio value of 19:56:0:0. This indicates that the leakage strength does not impact the concentration ratio at the extraction port, which is consistent with the law reflected in the following fig. 2.

These suggest that the numerical simulation results are consistent with the actual situation, thus confirming the validity of the numerical simulation results.

5 Results and discussion

5.1 Transport pattern analysis

To investigate the transport characteristics of two tracer gases (He and SF_6) during leakage, we simulated the leakage process in the condenser at leakage intensities of 0.77909310 and 0.07790931 kg/($m^3 \cdot s$). Fig. 2 displays the leaked gas flow rate variation at four outlets for He and SF_6 over time. Since the steam chambers on the left and right sides of the condenser are separated, the gas leaked from Zone 4 will not flow out through Outlets 1 and 2. Therefore, the flow rates at Outlets 1 and 2 shown in fig. 2, always remain at zero. Fig. 2 also reveals that the flow rate distribution at four outlets

is roughly similar. Most leaked gas tends to flow towards Outlet 3, while a small portion flows towards Outlet 4. The value of the flow rate at Outlet 4 is approximately one-seventh of that at Outlet 3.

Through comparison in fig. 2, it can be seen that the Outlet 3 flow rate process reaching a stable level under two different leakage intensifies presents two forms. When the tracer gas is He, it takes a long time (more than 10 seconds) to reach a stable state (fig. 2b). The other is in the form of a large slope, which can be quickly stabilized with only a short time (less than 3 seconds in fig. 2a). When the tracer gas is SF_6, the situation is similar. Under the two leakage intensities (figs. 2c and d), the time difference required for Outlet 3 flow rate to reach stability is also very large. In addition, it is noted that the time required for Outlet 4 flow rate to reach stability is almost the same, around 1.5 seconds. Based on these, it can be inferred that there are two distinct transport patterns in the leakage process.

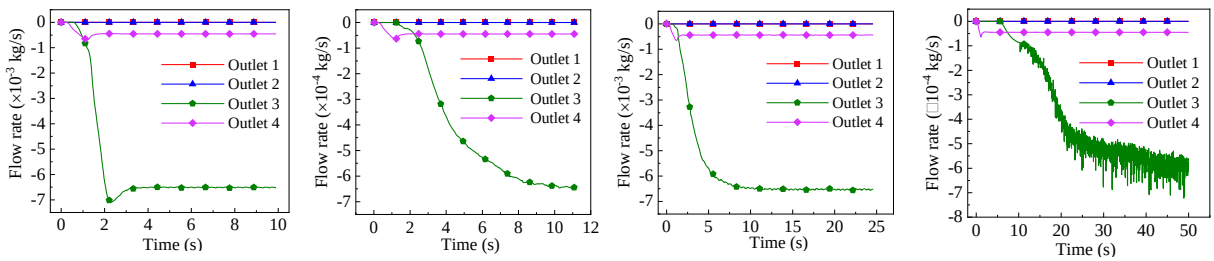

(a) He (b) He (c) SF_6 (d) SF_6

Fig. 2 Comparison of He and SF_6 leakage under two leakage intensities. The leakage intensity of (a) and (c) is 0.77909310 kg/(m^3·s), (b) and (d) is 0.07790931 kg/(m^3·s)

For analysis, the distribution of fluid pressure and velocity in Zones 3 and 4 are plotted in fig. 3 when the leakage intensity is 0.77909310 kg/(m^3·s) and the leaked gas is He. There is almost no pressure gradient near Outlet 3 in fig. 3a, which corresponds to the approximately no velocity near Outlet 3 in fig. 3b. And the pressure at the vicinity of Outlet 3 is almost at the lowest point. As a result, a small portion of the leaked gas will be able to flow out, while most of the leaked gas will stagnate near Outlet 3. To further analyze the subsequent flow of the leaked gas stagnating at Outlet 3, mass distribution diagrams of the leaked gas at intervals of 0.06 seconds are plotted in the figure of Appendix. It can be seen that the gas from the leakage position in Zone 4 continuously accumulates near Outlet 3. When the gas concentration reaches a sufficiently high level, it leaves Outlet 3 by diffusion.

However, such a phenomenon is not observed in Outlet 4. Due to the absence of cooling water in Zone 4, steam within that region is hardly condensed. The pressure gradient in Zone 4 is nearly small, as shown in fig. 3a. Additionally, the tube bundle has significant gas resistance, as indicated by the low and nearly uniform velocity within most areas in fig. 3b. Combining the two factors results in very little steam and leaked gas into Outlet 4. A noticeable pressure gradient is presented near the extraction port of Outlet 4 from fig. 3a. Thus, the little gas in Outlet 4 is all extracted instead of accumulating and diffusing out.

According to the above, the transport patterns of leaked gas through Outlet 3 involve flow and diffusion processes, while the transport through Outlet 4 only undergoes flow. Therefore, the transport patterns of leaked gas encompass two processes: 1) flow process and 2) diffusion process. All leaked gas has a flow process, but not all experience a diffusion process. The diffusion process refers to the

phenomenon that when the leaked gas accumulates to a specific concentration, the diffusion transport effect surpasses the flow transport effect and then leaves the outlet by diffusion-based transport.

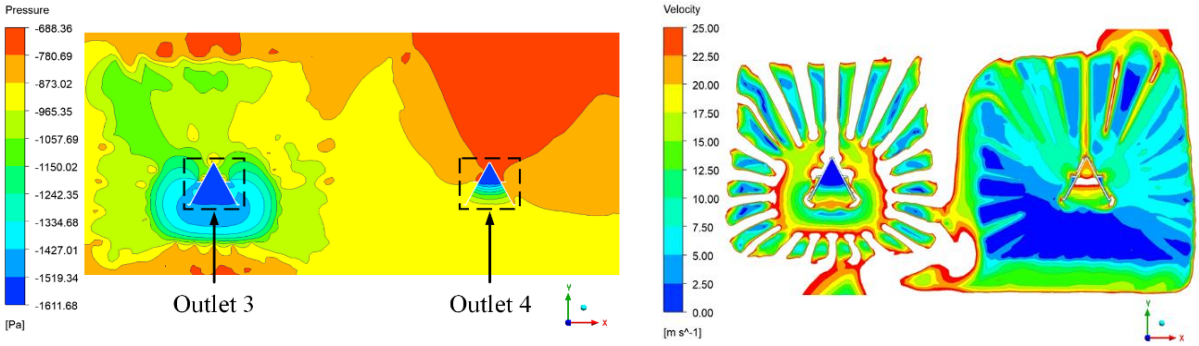

(a) (b)

Fig. 3 The distribution diagrams of (a) fluid pressure, and (b) fluid velocity in Zones 3 and 4.

5.2 Confirmation of diffusion process

Based on the research of section 5.1, it has been found that the transport pattern of leaked gas not only includes the flow process but also the diffusion process that occurs due to gas accumulation. This section will further confirm the diffusion process through theoretical analysis. According to the convective-diffusion equation for leaked gas [25], the leaked gas velocity is also almost zero when the steam velocity is zero. Therefore, both the source term and the convective term in the convective-diffusion equation are zero except for the leakage region. At this point, the equation transforms into Fick's law, as shown in eqs. (7) and (8).

$$J = -D\nabla c \tag{7}$$

$$\frac{\partial c}{\partial t} = -\nabla \cdot J \tag{8}$$

where J is the diffusion flux, representing the amount of substance diffusing through a unit area per unit time. D is the diffusion coefficient, c is the concentration, and t is time.

From the above equation, the diffusion rate (diffusion flux) of leaked gas is directly proportional to the diffusion coefficient under the same concentration difference. The time required to achieve the same concentration difference is inversely proportional to the diffusion coefficient. For estimating the diffusion coefficient of binary gases, Fuller proposed a general formula [30], as shown in eq. (9).

$$D = \frac{0.0101T^{1.75}\sqrt{\frac{1}{M_A}+\frac{1}{M_B}}}{P\left[(\sum v_A)^{1/3}+(\sum v_B)^{1/3}\right]^2} \tag{9}$$

where P is the total pressure of the gas. T is the temperature of the gas. M_A and M_B are the molar masses of components A and B, respectively. $\sum v_A$ and $\sum v_B$ are the molecular diffusion volumes of components A and B, respectively. The diffusion coefficient of A diffusing in B is consistent with the diffusion coefficient of B diffusing in A, so there is no longer a distinction between the form of diffusion coefficient.

Tab. 3 Gas property table.

Gas type	Molecular weight	Molecular diffusion volume (m^3)
He	4	2.67
SF_6	146	713
H_2O	18	13.1

According to eq. (9) and tab. 3, the diffusion coefficient of He in H_2O divided by the diffusion coefficient of SF_6 in H_2O is calculated to 6.67. Namely, the diffusion coefficient of He in steam is 6.67 times that of SF_6. Therefore, under the same concentration difference, the flow rate (diffusion flux) of He is 6.67 times that of SF_6. In other words, the time required for He to reach the same concentration difference is 1/6.67 times that of SF_6. To control the consistent diffusion coefficient, the timeline for He at Outlet 3 in fig. 2b is enlarged to 6.67 times the original. It is compared with the SF_6 flow rate curve at Outlet 3 in fig. 2d, as shown in fig. 4a.

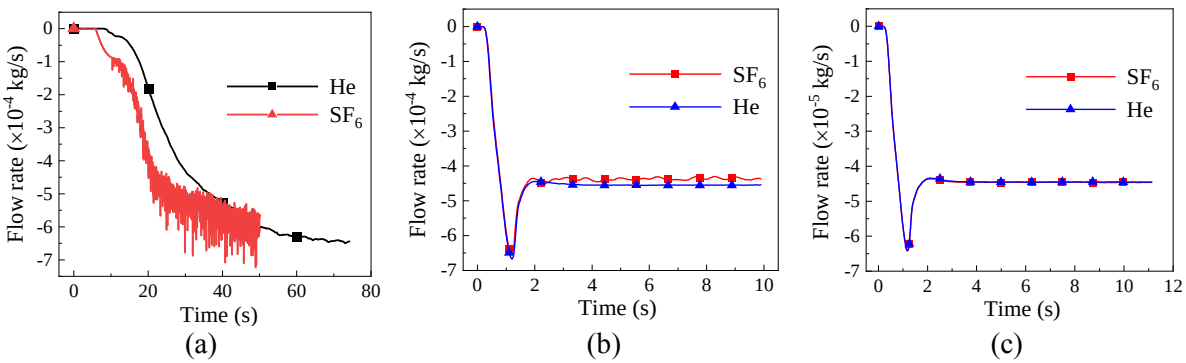

Fig. 4 The comparison of He and SF_6. (a) diffusion process;The flow rate at Outlet 4 when leakage intensities is (b) 0.77909310 kg/(m^3·s) and (c) 0.07790931 kg/(m^3·s).

It can be observed that the two curves roughly coincide. This means that when the diffusion coefficients are the same, the two leaked gases' transport process will become identical. That is, the transport of leaked gas at Outlet 3 is related to the gas diffusion coefficient, thus proving that the transport process includes the diffusion. Therefore, when only the species of leaked gas is changed, the flow rate curves of leakage gas hold the relationship: $f(D_1 \cdot t) = g(D_2 \cdot t)$, where the function of $f(x)$ and $g(x)$ is the flow rate curve of leaked gas in the diffusion coefficient of D_1 and D_2, repectively.

To confirm whether the transport pattern at Outlet 4 includes diffusion, the flow rate curves of He and SF_6 at Outlet 4 under two different leakage intensities in fig. 2 are plotted on the same graph for comparison, as shown in figs. 4b and c. The flow rate curves of the two gases with different properties exhibit consistent changes under both leakage intensities. This indicates that the leaked gas at Outlet 4 has undergone almost no diffusion process, only a flow process. Thus, this section further demonstrates that the transport pattern at Outlet 3 consists of the flow and diffusion processes, while the transport pattern at Outlet 4 only involves the flow process.

5.3 Effect of leakage intensity and gas species on transport

According to the four scenarios in fig. 2, the flow rates and time required for flow rate at Outlets 3 and 4 to reach a stable level are summarized in tab. 4. From tab. 4, the value of the flow rate for

stability is only directly proportional to the leakage intensity, regardless of the gas species. For example, under the leakage intensity of 0.77909310 kg/(m^3·s), the Outlet 3 flow rates for He and SF_6 are all -6.5e-3 kg/s, while the Outlet 4 flow rates are -4.6e-4 and -4.3e-4 kg/s. Under the leakage intensity of 0.07790931 kg/(m^3·s), the Outlet 3 flow rates for He and SF_6 are -6.4e-4 and -6.1e-4 kg/s, while the Outlet 4 flow rates are -4.6e-5 and -4.2e-5 kg/s, respectively. Therefore, no matter the transport patterns, the larger the leakage intensity, the greater the outlet flow rate for stability. Additionally, the species of leaked gas has almost no impact on the final outlet flow rate in both transport patterns.

From tab. 4, it also appears that the time required for the flow rate to reach a stable level is closely related to the transport pattern. In the case of the flow process (Outlet 4), the stabilization time for the flow rate is very short, completed within 2 seconds. However, the time will be much longer if there is a diffusion process (Outlet 3). According to tab. 4, when the leakage intensity is 0.77909310 kg/(m^3·s), it takes 10.7 seconds for the SF_6 flow rate at Outlet 3 to reach a stable level, while it takes 50 seconds when the leakage intensity is 0.07790931 kg/(m^3·s). This suggests that when the leakage intensity decreases, and the transport pattern includes diffusion, the diffusion process becomes more prominent, resulting in a longer time required for the flow rate to reach stability. However, when the transport pattern does not involve diffusion, the stabilization time for the flow rate does not change with the leakage intensity and gas species, as seen from the tab. 4.

Tab. 4 The flow rate of leaked gas at outlet reaching a stable value and the time required.

Leakage intensity ($kg·m^{-3}·s^{-1}$)	Position	He		SF_6	
		Flow rate ($kg·s^{-1}$)	Time (s)	Flow rate ($kg·s^{-1}$)	Time (s)
0.77909310	Outlet 3	-6.5e-3	3.0	-6.5e-3	10.7
	Outlet 4	-4.6e-4	1.5	-4.3e-4	1.7
0.07790931	Outlet 3	-6.4e-4	11	-6.1e-4	50
	Outlet 4	-4.6e-5	1.5	-4.2e-5	1.9

The effect of gas species on the diffusion process is further analyzed. Comparing the time required for Outlet 3 flow rate to reach stability at 0.77909310 kg/(m^3·s), it takes 10.7 seconds for SF_6 and 3 seconds for He, respectively. Considering that it is challenging to calculate the time for the flow process from the leakage point to Outlet 3, the time consumed at Outlet 4 (1.5 s) is used as a substitute. By calculation, the ratio of (10.7 s-1.5 s) to (3 s-1.5 s) is 6.13. This indicates that it requires 6.13 times longer for SF_6 than for He to achieve a flow rate stable in the pure diffusion process. According to section 5.2, the time consumed for SF_6 diffusion is 6.67 times that of He. By comparison, the difference between 6.67 and 6.13 is 8 %. The 8 % error is caused by inaccurate replacement for the time consumed during the flow process at Outlet 3 by Outlet 4. Therefore, it can be considered that the time required for the flow rate of the diffusion process to reach stability is inversely proportional to the gas diffusion coefficient.

In addition, notice many burrs on the flow rate curve at Outlet 3 in fig. 2d. These burrs are attributed to the combination of two factors: 1) the accumulation of leaked gas near the extraction port and 2) the disturbance from steam flow. When the gas's leakage intensity and diffusion rate (diffusion coefficient) are relatively small during diffusion, the leaked gas accumulates near the outlet, gradually reaching a specific concentration over time. This accumulation causes the gas to cover and almost

overflow the tube bundle in Zone 3, exposing it to the influence of steam flow. The presence of unstable flow factors, such as vortices in the condense, interferes with the leaked gas, resulting in disturbance. Due to the disturbance caused by the unstable steam flow, the flow curve displays continuous and significant oscillations. However, it is worth noting that when the gas leakage intensity or diffusion coefficient is large, the impact of these disturbances becomes less significant.

6 Conclusions

This paper investigates the leakage phenomenon and transport laws of two gases (He, SF_6) in the condenser tube bundle. The study indicates that the leaked gas includes two transport patterns: flow (in all gas transport processes) and diffusion (in parts of the gas transport process). In addition, the effects of leakage intensity and gas species on the leaked gas transport were also studied. The analysis are as follows:

(1) The gas flow process refers to the leaked gas being transported along with the steam flow. The outlet flow rate of leaked gas will rapidly decrease and quickly reach a stable level. The time required for stability is only related to the steam flow field. Gas diffusion refers to the process in which the leaked gas stagnates and accumulates in the extraction port under the combination of the small pressure gradient and large resistance, then diffuses out by concentration difference. Since the effect of gas transport through diffusion is much weaker than flow, the time required for the transport process, including diffusion, to reach stability is much longer than the pure flow process.

(2) The larger the leakage intensity for both transport patterns, the greater the outlet flow rate when reaching stability. However, the time required for outlet flow rate when reaching stability is closely related to the transport pattern. When the diffusion process is not included, the required time for stability will not change with the leakage intensity and gas species and is very short. When the diffusion process is included, the transport becomes complicated. The smaller the leakage intensity, the longer the required time. The required time for stability has a relation with gas species and is inversely proportional to the gas diffusion coefficient, which follows $f(D_1 \cdot t) = g(D_2 \cdot t)$.

(3) When using SF_6, the time required for the outlet flow rate to reach stability is 6-7 times longer than He. When the leakage intensity is low, the outlet flow rate of SF_6 will be more prone to high-frequency fluctuations or oscillations.

According to the above comparative study, SF_6 can be used instead of He as the tracer gas. Slightly different from the operation method when He is used, SF_6 may require 6-7 times the waiting time for stabilization than He.

Acknowledgements

This work was supported by the National Natural Science Foundation of China (U1905216), the Key Scientific and Technological Project of Henan Province (162102310152). Joint Research Project of Industry of China (H23-043). The computer simulation was supported by the high-performance computing platform of Henan Polytechnic University.

References

[1] Laskowski, R., *et al.*, A useful formulas to describe the performance of a steam condenser in off-design conditions, *Energy, 204* (2020), pp. 117910 https://doi.org/10.1016/j.energy.2020.117910

[2] Shin, D., *et al.*, Development of the thermal performance model using temperature gradient analysis for optimized design of steam surface condenser, *Int. J. Heat Mass Transfer, 163* (2020), pp. 120411 https://doi.org/10.1016/j.ijheatmasstransfer.2020.120411

[3] Zhao, X., *et al.*, Numerical simulation of micro-crack leakage on steam generator heat transfer tube, *Nucl. Eng. Des., 382* (2021), pp. 111385 https://doi.org/10.1016/j.nucengdes.2021.111385

[4] Xu, G., *et al.*, Remote characterization of ventilation systems using tracer gas and CFD in an underground mine, *Safety Sci., 74* (2015), pp. 140-149 https://doi.org/10.1016/j.ssci.2015.01.004

[5] Wu, Y., *et al.*, On-site measurement of tracer gas transmission between horizontal adjacent flats in residential building and cross-infection risk assessment, *Build. Environ., 99* (2016), pp. 13-21 https://doi.org/10.1016/j.buildenv.2016.01.013

[6] Olsen, D. B., *et al.*, Development of the tracer gas method for large bore natural gas engines—part I: method validation, *J. Eng. Gas Turbines Power, 124* (2002), 3, pp. 678-685 https://doi.org/10.1115/1.1454116

[7] Thekkuden, D. T., *et al.*, Failures and leak inspection techniques of tube-to-tubesheet joints: A review, *Eng. Failure Anal., 130* (2021), pp. https://doi.org/10.1016/j.engfailanal.2021.105798

[8] Rhino, K., *et al.*, Characterization and quantification of a CO2 and CH4 leakage experiment from a well into the carbonate vadose zone, *Int. J. Greenhouse Gas Control, 77* (2018), pp. 55-69 https://doi.org/10.1016/j.ijggc.2018.07.025

[9] Saegusa, T., *et al.*, Monitoring of helium gas leakage from canister storing spent nuclear fuel: Radiological consequences and management, *Nucl. Eng. Des., 382* (2021), pp. 111391 https://doi.org/10.1016/j.nucengdes.2021.111391

[10] Világi, F., *et al.*, Leakage estimation of the high-pressure and high-temperature natural circulation helium loop, *Ann. Nucl. Energy, 146* (2020), pp. 107584 https://doi.org/10.1016/j.anucene.2020.107584

[11] Li, X. M., *et al.*, Investigation on tip leakage flow characteristics of radial inflow micro turbine used in helium liquefying system, *Int. J. Refrig., 98* (2019), pp. 51-60 https://doi.org/10.1016/j.ijrefrig.2018.10.015

[12] Staf, M., *et al.*, Apparatus for testing He leakage through flange gaskets at elevated pressure and temperature, *Prog. Nucl. Energy, 139* (2021), pp. 103831 https://doi.org/10.1016/j.pnucene.2021.103831

[13] Qin, H., *et al.*, Experimental investigation on flow and heat transfer characteristics of He-Xe gas mixture, *Int. J. Heat Mass Transfer, 192* (2022), pp. 122942 https://doi.org/10.1016/j.ijheatmasstransfer.2022.122942

[14] Qin, S., *et al.*, Models of helium enrichment in helium-rich gas reservoirs of petroliferous basins in China, *Nat. Gas Ind. B., 10* (2023), 2, pp. 130-139 https://doi.org/10.1016/j.ngib.2023.01.006

[15] Park, I. W., *et al.*, Degradation of condensation heat transfer on a vertical cylinder by a light noncondensable gas mixed with air-steam mixtures, *Int. Commun. Heat Mass Transfer, 130* (2022), pp. 105779 https://doi.org/10.1016/j.icheatmasstransfer.2021.105779

[16] Bai, J., *et al.*, Analysis of SF6 contact based on QPSO-SVR, *Energy Rep., 9* (2023), pp. 425-433 https://doi.org/10.1016/j.egyr.2023.03.020
[17] Sun, H., *et al.*, Simulation and experimental study on the degradation of the greenhouse gas SF6 by thermal plasma, *Environ. Res., 216* (2023), pp. 114411 https://doi.org/10.1016/j.envres.2022.114411
[18] Rigby, M., *et al.*, History of atmospheric SF 6 from 1973 to 2008, *Atmos. Chem. Phys., 10* (2010), 21, pp. 10305-10320 https://doi.org/10.5194/acp-10-10305-2010
[19] Korlapati, N. V. S., *et al.*, Review and analysis of pipeline leak detection methods, *Journal of Pipeline Science and Engineering, 2* (2022), 4, pp. 100074 https://doi.org/10.1016/j.jpse.2022.100074
[20] Liang, J., *et al.*, Data-driven digital twin method for leak detection in natural gas pipelines, *Comput. Electr. Eng., 110* (2023), pp. 108833 https://doi.org/10.1016/j.compeleceng.2023.108833
[21] Zhang, Z., *et al.*, MFCC- LSTM framework for leak detection and leak size identification in gas-liquid two-phase flow pipelines based on acoustic emission, *Measurement, 219* (2023), pp. 113238 https://doi.org/10.1016/j.measurement.2023.113238
[22] Idachaba, F., Tomomewo, O., Surface pipeline leak detection using realtime sensor data analysis, *Journal of Pipeline Science and Engineering, 3* (2023), 2, pp. 100108 https://doi.org/10.1016/j.jpse.2022.100108
[23] Juan, D., Hai-Tao, Z., Numerical simulation of a plate-fin heat exchanger with offset fins using porous media approach, *Heat Mass Transfer, 54* (2017), 3, pp. 745-755 https://doi.org/10.1007/s00231-017-2168-3
[24] Abe, S., *et al.*, Density stratification breakup by a vertical jet: Experimental and numerical investigation on the effect of dynamic change of turbulent schmidt number, *Nucl. Eng. Des., 368* (2020), pp. 110785 https://doi.org/10.1016/j.nucengdes.2020.110785
[25] Zhang, J., *et al.*, A hybrid mixed finite element method for convection-diffusion-reaction equation with local exponential fitting technique, *Appl. Numer. Math., 189* (2023), pp. 23-38 https://doi.org/10.1016/j.apnum.2023.03.009
[26] Davies, W. A., *et al.*, Heat transfer and flow regimes in large flattened-tube steam condensers, *Appl. Therm. Eng., 148* (2019), pp. 722-733 https://doi.org/10.1016/j.applthermaleng.2018.11.079
[27] Zhang, C., *et al.*, The Numerical and Experimental Study of a Power Plant Condenser, *J. Heat Transfer, 115* (1993), 2, pp. 435-445 https://doi.org/10.1115/1.2910696
[28] Cavalcanti, L. L. F., *et al.*, Determination of CO2 solubility in Perna perna mussel and analysis of the suitability of the ideal and non-ideal gas models, *Chemical Thermodynamics and Thermal Analysis, 7* (2022), pp. 100075 https://doi.org/10.1016/j.ctta.2022.100075
[29] Ahn, S.-H., *et al.*, Unsteady prediction of cavitating flow around a three dimensional hydrofoil by using a modified RNG k-ε model, *Ocean Eng., 158* (2018), pp. 275-285 https://doi.org/10.1016/j.oceaneng.2018.04.005
[30] Fuller, E. N., *et al.*, New method for prediction of binary gas-phase diffusion coefficients, *Ind. Eng. Chem., 58* (1966), 5, pp. 18-27 https://doi.org/10.1021/ie50677a007

Paper submited: 01.09.2023
Paper revised: 06.11.2023
Paper accepted: 18.11.2023